JOURNAL OF SPACECRAFT AND ROCKETS
Vol. 35, No. 3, May–June 1998

Experimental Investigation of Super- and Hypersonic Jet Interaction on Missile Configurations

Julius Brandeis* and Jacob Gill*
RAFAEL, Ministry of Defense, Haifa 31021, Israel

An experimental investigation of jet interaction on configurations with lifting surfaces is presented. The experiments were carried out at supersonic Mach numbers of 2, 3.3, and 4.5 and at the hypersonic Mach number of 8. The test model was an ogive-cylinder body with interchangeable lifting surfaces that can be mounted at various locations along the body. Several body–surface combinations were tested representing wing, tail, wing plus tail, and strake configurations. In some cases, the presence of the surfaces resulted in large force and/or moment amplification due to the interaction of the jet-induced flowfield with the planar surfaces. Large amplification factors were obtained at zero angle of attack for some configurations even at the low Mach number of 2. In contrast, for similar tests using body of revolution without additional surfaces, only small force amplification, at best, could be obtained at small angles of attack. The force amplification was also shown to vary inversely with jet pressure. For low values of the jet stagnation pressure, amplification factors in excess of 2 were obtained. The interaction moments could be used to obtain an additional, aerodynamic, lifting force, which for some configurations can further increase the control force.

Nomenclature

A	= jet nozzle exit area, mm^2
C_m	= pitching moment coefficient
DC_m	= interactive pitching coefficient
d	= body diameter equal to reference length, mm
F	= normal force measured by the balance, kg
F_i	= normal force due to interaction effects, kg
F_j	= jet thrust corrected for tunnel static pressure, kg
F_{js}	= jet thrust at $M = 0$ (no wind), kg
K	= jet-force amplification factor
K_z	= normal amplification at side slip angle
l	= body length, cm
M	= pitching moment; reference x of 125 mm, kg · cm
M_∞	= freestream Mach number
m	= jet mass flow rate, kg/s
P_{ej}	= jet exit pressure, psi
P_s	= freestream static pressure, kg/cm^2
P_{0j}	= jet stagnation pressure, psi
P_{0t}	= freestream stagnation pressure, kg/cm^2
Q_j	= jet dynamic pressure, kg/cm^2
Q_t	= freestream dynamic pressure, kg/cm^2
Re	= Reynolds number, 1/m
T_{ej}	= jet exit temperature, K
T_{0j}	= jet stagnation temperature, K
T_{0t}	= freestream stagnation temperature, K
T_∞	= freestream static temperature, K
XCP_i	= interaction center of pressure location (in terms of body diameter), $[d]$
X_{cg}	= moment reference, mm
α	= angle of attack, deg
β	= angle of side slip, deg

Introduction

THE influence of size and location of planar surfaces on the amplification of jet thrust is investigated for several supersonic and hypersonic Mach numbers and for various jet injection pressures. Such force amplification leads to a larger control force for a given jet thrust.

Received Aug. 7, 1997; presented as Paper 97-3723 at the AIAA Atmospheric Flight Mechanics Conference, New Orleans, LA, Aug. 11–13, 1997; revision received Dec. 23, 1997; accepted for publication Dec. 29, 1997.

*Research Engineer, Aeronautical Systems Department. Member AIAA.

When a jet is injected into the super/hypersonic freestream, a complex flowfield is created, comprising various shock wave patterns. The surface pressures induced by the interaction can, under certain conditions, lead to an increase in the direct force control. Such force amplification has been reported in a number of prior publications for two-dimensional and axisymmetric (body-alone) configurations.[1–4]

The mechanism for this force amplification is as follows. The jet issuing into the super/hypersonic freestream acts as an obstacle to the flow and produces a strong shock wave, called jet bow shock. The effect of this detached shock is a pressure rise, which envelopes the nozzle. Downstream of the nozzle, the surface pressures are generally lower than ambient in supersonic flows but are reported to be higher than ambient at hypersonic speeds.[2] The disturbance also propagates upstream through the boundary layer, creating a wedge-like region of separated flow ahead of the jet, with its separation shock and elevated surface pressure.

In our past research on jet interaction[5] an ogive-cylinder configuration similar to the present model but without any lifting surfaces was utilized. The measured force amplification factor K was generally low at zero angle of attack but was found to be relatively high at positive angles of attack. Very significant pitching moments due to the jet interaction were measured. At high Mach numbers ($4.5 < M < 10$), force amplification factors greater than unity were obtained with zero angle of attack. For the low Mach number ($M = 2$) and at $\alpha = 0$ deg, K was significantly less than unity, indicating a net loss in the available control force. In all cases, the force amplification obtained was much smaller than that reported by Spaid[2] for two-dimensional interaction on flat plates. This major difference between the three-dimensional and the planar results can be explained by noting that the bow shock tends to wrap around the circular body, as shown experimentally in Refs. 5 and 6, thus producing high pressure on the underside of the body and reducing the jet amplification factor. Hsieh and Wardlaw[7] presented an accurate, viscous numerical solution that clearly shows the jet-induced, high pressures acting on the underside of the circular body.

By placing planar surfaces in regions subjected to high pressures from the jet interaction, an additional control force can be obtained. Conversely, the same surface subjected to low pressure will result in a negative contribution to the control force. The induced control moments can be large as well. The possibility of obtaining force amplification due to the presence of such surfaces was reported in general terms in Ref. 8. The force amplification due to the surfaces was shown to be a function of their mounting location. Very recently Srivastava[9] reported moderate force amplification due to planar surfaces at $M = 3.94$.

The amplification factor, therefore, can be increased by use of planar surfaces, as already discussed, or by mounting the injection nozzle at the aft end of the body, thereby eliminating the downstream low-pressure region.[3] The latter method is particularly appropriate for low supersonic Mach numbers, where the downstream pressures are low.

Another effect that may be very useful for vehicle control is the induced moment due to the upstream and the downstream interaction. As noted, the upstream overpressure and the downstream underpressure regions produce a nose-down moment couple about the injection location. The resulting angle of attack gives rise to an aerodynamic force that acts in the same direction as the jet thrust force and can serve to increment further the control force. If a specific body attitude is to be maintained, then these moment-induced effects can be undesirable.

Experimental Setup and Procedure

Description of the Model and Its Parts

The wind-tunnel test model consists of a circular cross-section body and three sets of lifting surfaces. The body was built up around the 50-mm-diam midsection including balance mount, jet plenum, and mounting space for the interchangeable jet nozzles. The model's center section and the special balance with concentric gas supply line for the jet were used in previous experiments.[5] A sharp, ogive-shaped nose section of $l/d = 2$ and a cylindrical $l/d = 3$ afterbody were mounted to the midsection for the total model length of 290 mm and $l/d \sim 6$ (see Fig. 1). The circular, sonic nozzle center point is located 125 mm from the nose tip and has a nominal diameter of 5 mm and throat area of 19.6 mm^2. The model was mounted in the tunnel in such orientation that for positive α the jet is on the leeward side.

The novel elements in the present experiments are the planar surfaces designed for mounting on the body at various lengthwise locations (see Fig. 1). Note the lifting surfaces all have the same exposed semispan of 25 mm and the leading-edge sweep angle of 45 deg.

The body-lifting surface configurations shown in Fig. 1 were tested.

1) Configuration 1 has forward wing location. The root leading edge is located 100 mm from the nose tip.

2) Configuration 2 has tail location. The root leading edge of each tail surface is now located 220 mm from the nose tip.

3) Configuration 1 + 2 has a wing–tail arrangement mounted together. The corresponding surfaces are mounted in the same locations as for configurations 1 and 2.

4) Configuration 3 simulates the presence of strakes spanning 65% of the body's length. The root leading edge is positioned 100 mm from the nose tip.

5) Configuration 4 has wings mounted 30 mm downstream of the mounting point for configuration 1. The root leading edge is located 130 mm from the nose tip.

6) The body-alone configuration (no lifting surfaces) was tested as a reference configuration for comparison.

Balance

A four-component sting balance with coaxial air supply passage (for jet injection) was used. This balance, manufactured especially for the previous experiments with side-jet injection, measures two forces and two moments (pitch and yaw) but does not measure the axial force and the rolling moment. Within the balance there is a concentric passage through which the compressed gas is supplied to the jet plenum within the model. The balance and the model mounting system were designed to eliminate any influence of the air supply on the balance measurements.

Test Facilities and Equipment

The supersonic experiments were carried out at the Israel Aircraft Industries (IAI) trisonic wind-tunnel facility (4 × 4 ft test section) at Mach numbers of 2, 3.3, and 4.5. Another, similar, series of experiments was carried out in the IAI hypersonic wind-tunnel facility at $M = 8$. These two facilities differ greatly in the range of Mach and Reynolds numbers, as shown in Table 1. The injectant gas used in the supersonic experiments was nitrogen, whereas the gas in the hypersonic tests was air from the pressure line. The jet mass flow

Table 1 Flow conditions for wind tunnels used

Mach	P_{0t}, kg/cm^2	P_s, kg/cm^2	Q_t, kg/cm^2	T_{0t}, K	Re, 10^6 m^{-1}
2.0[a]	1.95	0.252	0.698	306	22.3
3.3[a]	5.46	0.105	0.730	307	31.8
4.5[a]	15.2	0.057	0.745	306	29.8
8.0[b]	26.0	0.0026	0.120	725	5.87

[a]IAI trisonic wind tunnel. [b]IAI hypersonic wind tunnel.

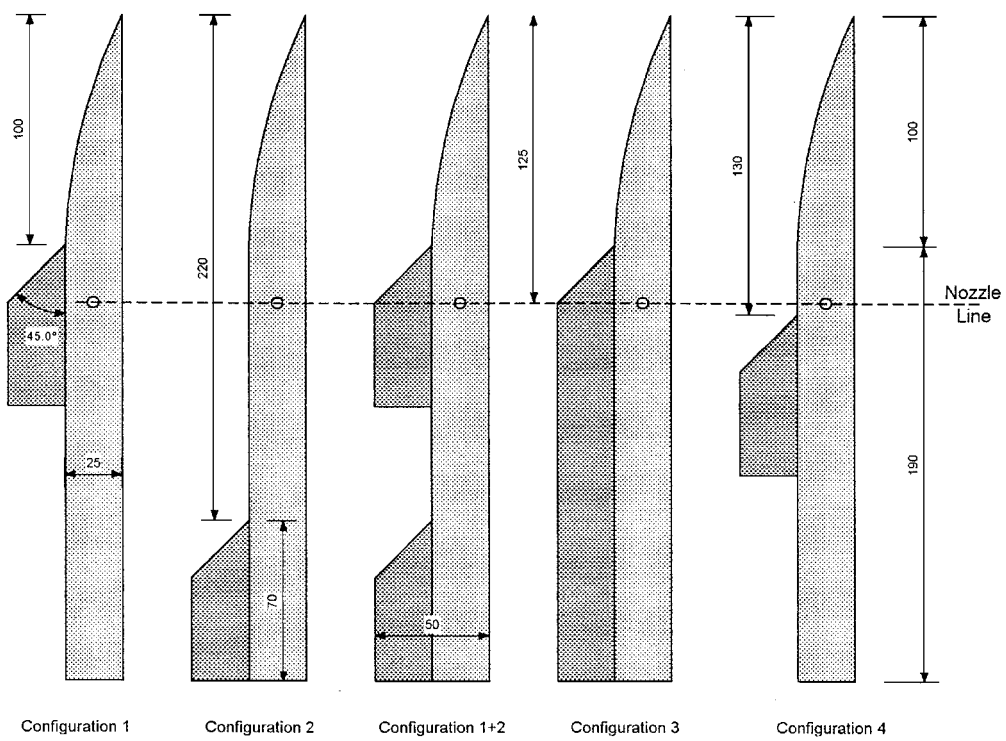

Fig. 1 Configurations schemes.

rate was determined from a calibrated nozzle in the supply line. Jet stagnation pressure was determined from measurements within the jet stagnation chamber (plenum) and from a calibrated nozzle or orifice plate installed in the gas supply line. The stagnation pressure measured in the plenum conformed fairly well with the line measurement, indicating that the plenum within the model can be assumed to be a stagnation chamber.

In all tests, schlieren flow imagery was obtained and recorded using a video camera. In the hypersonic facility, where the flow density is very small, obtaining acceptable quality schlieren visualization was a problem.

Experimental Procedure

Series of experiments were carried out at different Mach numbers and with various model configurations. To evaluate the jet interaction effects, the following three types of experiments were needed for each configuration.

1) Calibration experiment was to measure the jet thrust force at specified stagnation pressure (no wind in the tunnel). This thrust force was corrected for the actual freestream static pressure conditions prevailing in the relevant wind-on experiment.

2) Aerodynamic experiment was to measure the forces and moments of a configuration at the desired Mach number but without activating the jet. The forces and moments measured are purely due to the configurations' aerodynamics.

3) Jet experiment with injection was conducted at the desired Mach number and with full-angle-of-attack sweep. The measured data include the direct jet contribution, the jet interaction contribution, and the configuration aerodynamics contribution.

Most experiments were performed at a set Mach number and jet injection pressure while the angle of attack was continuously varied. Other experiments were performed at a set Mach number and angle of attack but with injection pressure as the control variable. In addition, the effect of side slip angle β on the interaction was investigated at $M = 2$.

The boundary layer was not tripped by any artificial means. It was assumed fully turbulent in the supersonic experiments, but some laminar flow is expected in the hypersonic tests.

Data Reduction and Interpretation

It is convenient to define the interaction amplification factor K as the integrated interaction pressures together with the jet thrust, divided by the jet thrust adjusted to the freestream static pressure:

$$K = \frac{F_i + F_j}{F_{js}} \tag{1}$$

Note that F_i and F_j are not measured directly. Rather, $F_j + F_i$ is derived by subtracting the force measured in the aerodynamic experiment from that measured in the corresponding jet experiment. In effect, this is equivalent to

$$K = \frac{F_{\text{jet on}} - F_{\text{jet off}}}{F_{js}} \tag{2}$$

F_j is, in principle, equal to F_{js}.

The moment coefficient due to interaction may be expressed as the difference between the pitching moment coefficient measured on a configuration with and without the jet:

$$DC_m = (C_m)_{\text{jet on}} - (C_m)_{\text{jet off}} \tag{3}$$

These moment coefficients are centered around the nozzle location ($x = 125$ mm), so that the jet itself does not contribute to the moment, and, therefore, DC_m is the pure interaction contribution to the pitching moment coefficient.

Another way to present the moment interaction is by examining the shift in the center of pressure caused by the interaction. The straightforward way to implement this is as follows:

$$XCP_i = (M_{\text{jet on}} - M_{\text{jet off}})/(F_{\text{jet on}} - F_{\text{jet off}})/d \tag{4}$$

The numerator in Eq. (4) is the pure interaction moment, whereas the denominator represents the combination $F_j + F_i$. Equation (4), therefore, calculates the axial location where the combination of the jet and the interaction forces act, in terms of body diameter (relative to the center of moments, which is the jet nozzle). The XCP_i definition in Eq. (4) is used as a characteristic jet interaction moment length scale for data presentation because it is a better measure of the interaction moment effect then DC_m.

Experimental Results

The results are presented in terms of parameters chosen to quantify the jet interaction effects. These are the amplification factor K and the interactive force center of pressure XCP_i, defined in Eqs. (2) and (4), respectively. All moment-related parameters are based on the reference location corresponding to the assumed X_{cg} at the nozzle location (125 mm from the nose point).

Supersonic Experiments

In Fig. 2 force amplification factor is plotted as a function of angle of attack for the five configurations with lifting surfaces and for the body-alone configuration. These results were obtained at $M = 4.5$. The stagnation pressure was approximately 550 psi. It is clearly seen that, for all configurations except for configuration 2 (tail), the force amplification at zero angle of attack is much higher than for the body alone.

For configuration 2 the results are quite similar to the body-alone case, especially at positive angles of attack. This implies that the tail does not experience significant pressure changes due to the jet flowfield at $M = 4.5$ except at negative angles of attack, for which there appear to be losses in control force relative to the body-alone case. The best force amplification ($K \sim 1.5$) at zero angle of attack is for the forward-wing configuration 1. A 30-mm aft displacement of the wing in configuration 4 reduces K to 1.35, showing the importance of the surface's location with respect to the jet shock. The optimal location is, therefore, dependent on the Mach number. Configurations 3 (strakes) and configuration 1 + 2 (wing plus tail) give very similar results at positive angles of attack. For these cases $K = 1.4$, which is very similar to the result for configuration 1. Noteworthy are the differences in the angle-of-attack dependence for these configurations. For configuration 1 + 2 (wing and tail), the amplification factor is insensitive to the angle of attack. For all other cases, K increases with increasing angle of attack. At positive angles of attack, the differences between the configurations decrease substantially.

The interaction center of moment XCP_i, shown in Fig. 2, reflects the interactive pitching moment behavior. Large interactive pitch-down moments at negative α are experienced, not surprisingly, for configurations 3 and 2, having surfaces extending to the tail of the

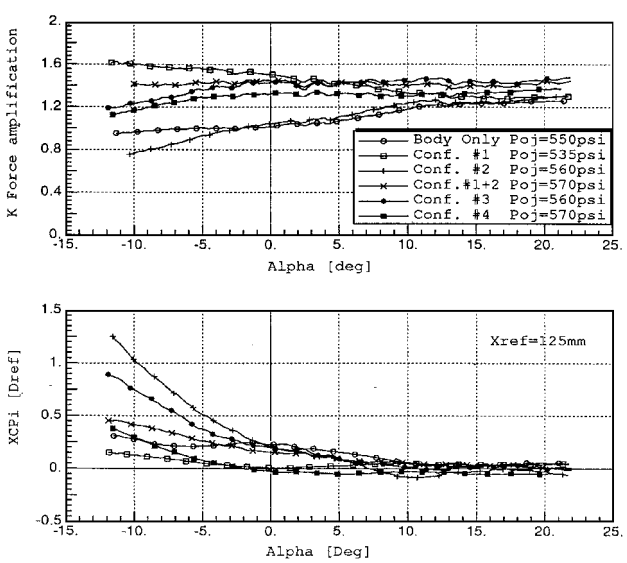

Fig. 2 Force amplification factor and interaction center of pressure vs angle of attack at Mach = 4.5, m = 0.18 kg/s, P_{0j}/P_{0t} = 2.6, and Q_j/Q_t = 20.

configuration. XCP_i is small for all configurations with the exception of configurations 2 and 3, for which it exceeds $0.5d$ for large negative α. Positive XCP_i is the result of nose-down pitching moment produced by interaction pressures acting on the low rear part of the configuration.

The force interaction at $M = 2$ differs from the higher Mach number cases. Here, degradation of control force effectiveness due to interaction can be expected on the basis of our previous studies[5] and other published results, i.e., Ref. 8. In Fig. 3 the force amplification results are presented for $M = 2$. Configurations 1, 2, and 3, as well as the reference body-alone case, are considered. Note that the results for configuration 1 are for the jet stagnation pressure of 515 psi, whereas the other results plotted were obtained with P_{0j} of 400 psi, approximately.

For configuration 1 (wings), $K > 1$ was obtained at all angles of attack. For all other cases shown, values of K significantly smaller than unity were obtained, especially at negative values of the angle of attack. In this region, configuration 2 (tail) shows a decrease in control force compared to the body-alone case, indicating the negative contribution of the tail. As in the $M = 4.5$ comparison, configuration 1 gave the largest values of K. The difference between configuration 1 and other configurations is much greater for $M = 2$ than for $M = 4.5$. Note that, if P_{0j} used in this case was 100 psi lower (equal to the other cases presented), the values of K for configuration 1 would be about 10% higher on the basis of transient data, which will be presented in Fig. 4.

The interactive center of pressure parameters (shown in Fig. 3) illustrate that for $M = 2$ the interaction gives rise to generally large nose-down pitching moment. The exception is configuration 1, which is consistent with the prior, higher Mach number, results in its low pitching moment coefficients and their insensitivity to the angle of attack. The values of XCP_i (Fig. 3) are large for configurations 2 and 3, especially at negative α. The variation of XCP_i for these configurations is irregular. This is caused by the large pitching moments and small jet-induced forces characteristic for these configuration at low Mach numbers.

In Fig. 4 the force amplification coefficient K is plotted as a function of the jet stagnation pressure normalized by the tunnel stagnation pressure (P_{0j}/P_{0t}) for supersonic Mach numbers (2, 3.3, and 4.5) at zero angle of attack. All of these results refer to configuration 1 with the wings in the forward position. It is seen that the results for different Mach numbers are fairly consistent. The maximum amplification factor $K \sim 2$ is obtained for the value of jet/freestream stagnation pressure ratio of unity. For greater and for smaller jet stagnation pressures, the amplification factor decreases.

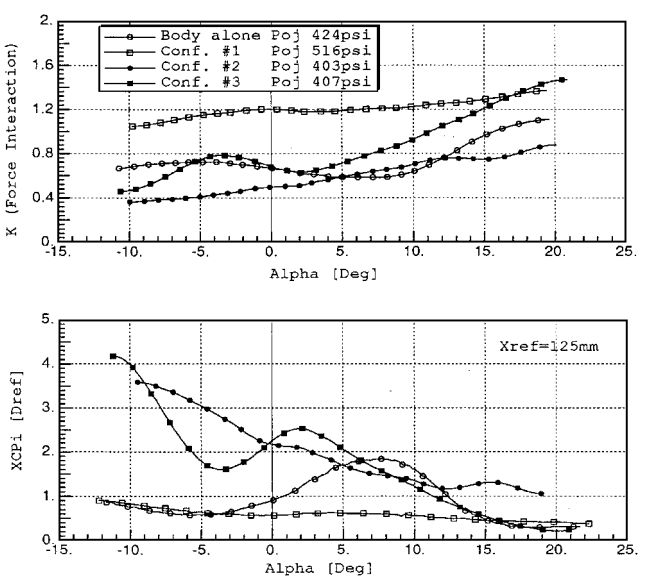

Fig. 3 Force amplification factor and interaction center of pressure vs angle of attack at Mach = 2.0: P_{0j} at 500 psi, m = 0.17 kg/s, P_{0j}/P_{0t} = 20, and Q_t/Q_j = 21; and P_{0j} at 400 psi, m = 0.13 kg/s, P_{0j}/P_{0t} = 15, and Q_j/Q_t = 15.

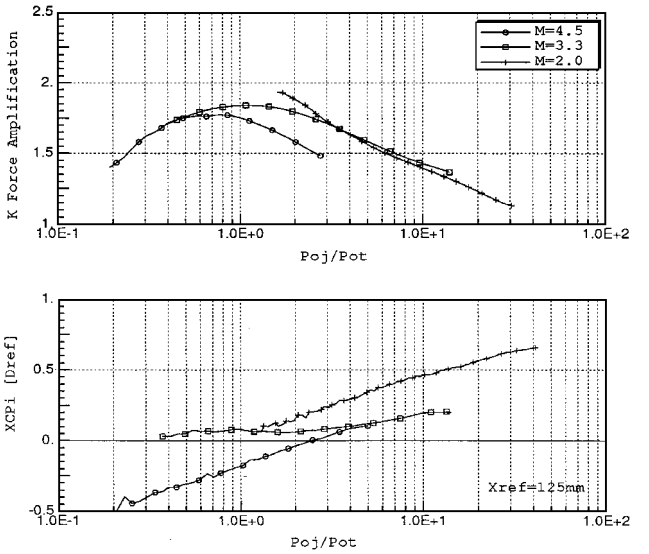

Fig. 4 Transient force amplification factor and interaction center of pressure vs stagnation pressure ratio for configuration 1 at three supersonic Mach numbers.

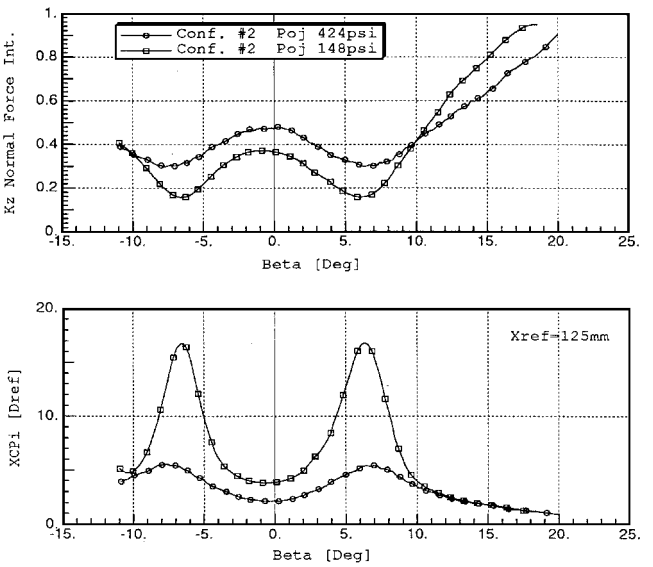

Fig. 5 Normal force amplification and interaction center of pressure vs side slip angle for the body–tail configuration at $M = 2$ and $\alpha = 0$ deg: P_{0j} at 150 psi, m = 0.05 kg/s, P_{0j}/P_{0t} = 5, and Q_t/Q_j = 6; and P_{0j} at 400 psi, m = 0.13 kg/s, P_{0j}/P_{0t} = 15, and Q_j/Q_t = 15.

It is noteworthy that for given P_{0j}/P_{0t} the highest amplification factors were obtained for the lowest Mach number, $M = 2$. With body alone, values of $K < 1$ are obtained. Apparently, at $M = 2$ the forward wing surfaces are able to capture effectively the jet bow shock as it spreads in the lateral direction.

The dependence of XCP_i on the jet pressure at $\alpha = 0$ deg appears in Fig. 4. It may be seen that for configuration 1, the variation of XCP_i with jet pressure is small, considering the range of pressures displayed.

These results were also replotted using the ratio of jet-to-freestream momentum as the independent variable. Q_j/Q_t, as will be recalled, is an indication of the jet penetration ability. The resulting plots were qualitatively similar to those in Fig. 4, but the correlation between different Mach number cases was better in Fig. 4, thus justifying the present selection.

Effects Due to Side Slip Angle at $M = 2.0$

The influence of the side slip angle β on the interaction component of the normal force (in terms of normal force amplification factor K_z) and on the interaction pitching moment (nominal $\alpha = 0$ deg) is shown in the graphs presented in Fig. 5. The configuration examined

is the body–tail configuration 2. The first feature noted in these results is their symmetry around $\beta = 0$ deg. The normal force amplification factor K_z has a local maximum there and decreases to a minimum value at $|\beta| \sim 7$ deg. From there, K_z increases uniformly with increasing $|\beta|$. For $\beta = 0$ deg and $P_{0j} = 424$ psi, the value of K_z is entirely consistent with the result at $\alpha = 0$ deg in Fig. 3.

The values of K_z obtained for $P_{0j} = 148$ psi are lower than for the preceding case but show the same dependence with β. The XCP_i exhibits similar sinusoidal β variation noted for K_z; the peak values are exaggerated for higher pressure value due to the small interaction forces. At the points where K_z is at a maximum, the interaction XCP_i is smallest in magnitude, and where K_z is at its minimum value, XCP_i is maximum in magnitude. The pitching moment is nose down for the entire range of β. This is consistent with low jet-induced pressures acting on the tail planes in $M = 2$ flow, as noted earlier.

The corresponding side force and moment due to β were negligibly small by comparison. In contrast with the pitch-plane results, the side force and moments were antisymmetric about $\alpha = 0$ deg (sine wave).

Hypersonic Experiments

The $M = 8$ experiments were conducted under test conditions different from those in the supersonic experiments. The jet mass flow rate had to be kept down in order not to affect the tunnel operating conditions. Consequently, the jet stagnation pressures and P_{0j}/P_{0t} were one to two orders of magnitude lower than the corresponding supersonic values, but the Q_j/Q_t range was of the same order of magnitude.

Plots of K vs angle of attack for the various configurations obtained at $M = 8$ and with $P_{0j} = 28$ psi are presented in Fig. 6. Configurations 1, 2, 3, 1 + 2, and body alone are shown. For all cases shown in Fig. 6, large values of the amplification parameter are obtained, compared to the values shown for the supersonic cases. It is immediately seen that for configuration 3 (strakes) the highest values of K ($K = 2.6$) are obtained. Next is configuration 1 + 2 (body plus wing plus tail) with $K \sim 2$, and configuration 1 (wings), shown best at supersonic speeds, is only third best, with $K \sim 1.7$. It is important to note the difference in total control force for configurations 1 and 3 is almost equal to the net jet thrust. Configuration 2 (tail) is seen to have an advantage over the body alone, which means that at $M = 8$ the tail contribution to the interaction force is in the direction of the jet thrust. The superior performance of strakes and body plus wing plus tail due to the high pressures experienced by the tail illustrates the qualitative difference between hypersonic and supersonic jet interaction.

The corresponding results for XCP_i are shown in Fig. 6. The interaction moments at $M = 8$ are relatively small and well ordered. For configurations 2, 3, and body alone, nose-up moments are caused by interaction, indicating a force contribution due to tail planes in the same direction as the jet thrust. This was not seen at supersonic speeds. For the body–wing configuration, uniform nose-down moments are seen, similar to the supersonic results. In contrast with the supersonic results, the pitching moment data rule out any use of the aerodynamic force supplement because such force would act in the direction opposite to the direction of the maneuver for configurations other than configuration 1.

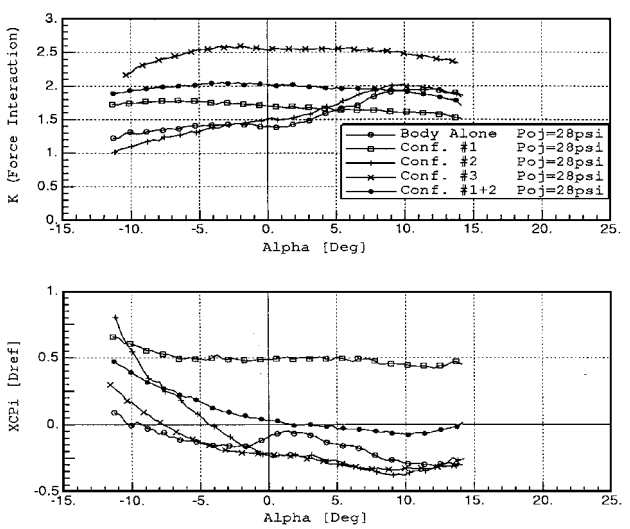

Fig. 6 Force amplification factor and interaction center of pressure vs angle of attack at $M = 8$, $m = 0.009$ kg/s, $P_{0j}/P_{0t} = 0.08$, and $Q_j/Q_t = 6$.

Table 2 Summary of force amplification K for case considered, $\alpha = 0$ deg, $Q_j/Q_t \sim 15$

	Force amplification, K		
Mach	2.0	4.5	8.0
Body	0.7	1.0	1.4
Body–wing (configuration 1)	1.2	1.5	1.7
Body–tail (configuration 2)	0.5	1.0	1.5
Body–wing–tail (configuration 1 + 2)	——	1.4	2.0
Body–strake (configuration 3)	0.7	1.4	2.6
Body–midwing (configuration 4)	——	1.3	——

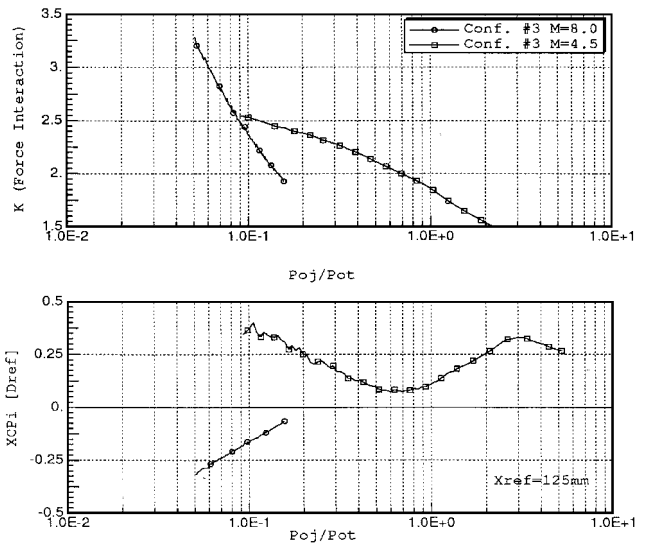

Fig. 7 Transient force amplification factor and interaction center of pressure vs stagnation pressure ratio: comparison for body–strake configuration at $M = 4.5$ and $M = 8$.

Results from the pressure transient experiment for the configuration with strakes are presented in Fig. 7 as a function of the jet-to-tunnel stagnation pressure ratio P_{0j}/P_{0t}. Figure 7 includes comparison with the corresponding results at $M = 4.5$.

As seen from Fig. 7, both K and XCP_i show steady decrease in magnitude with rising jet pressure. At $M = 8$, $K > 3$ was obtained at the low end of the injection pressures. At $M = 8$ there appears to be no maximum value of K within the range of the P_{0j} considered. Such a maximum was observed in the supersonic experiments with configuration 1, as seen in Fig. 4. The plots of K vs P_{0j}/P_{0t} for configuration 3 at $M = 8$ and 4.5 in Fig. 7 reveal that the slopes of the two graphs differ greatly, indicating perhaps that P_{0j}/P_{0t} may not be the appropriate nondimensional parameter. Note that highest K values for the $M = 8$ case occur for values of P_{0j}/P_{0t} lower than those for the $M = 4.5$ case.

The XCP_i data, presented in Fig. 7, show nose-up pitching moment at $M = 8$ for the entire jet pressure range (in contrast to the nose-down moment for $M = 4.5$). The XCP_i magnitude is quite small, not exceeding 0.3 diameters for both Mach numbers.

Tables 2 and 3 compare the main features of the interaction for various configurations at the different Mach numbers. These results are for high injection pressures, corresponding to the values of the dynamic pressure ratio $(Q_j/Q_t) > 15$.

Flow Visualization at $M = 4.5$

Schlieren photographs of the supersonic interaction flowfield for configuration 1 are presented in Fig. 8, showing the main features of

Table 3 Summary of XCP_i for case considered, $\alpha = 0$ deg, $Q_j/Q_t \sim 15$

	$\lvert XCP_i \rvert$,[a] $[d]$		
Mach	2.0	4.5	8.0
Body	0.9 ↓[b]	0.25 ↓	0.10 ↑[c]
Body–wing (configuration 1)	0.5 ↓	0.00	0.50 ↓
Body–tail (configuration 2)	2.2 ↓	0.20 ↓	0.25 ↑
Body–wing–tail (configuration 1 + 2)	——	0.15 ↓	0.00
Body–strake (configuration 3)	2.2 ↓	0.20 ↓	0.25 ↑
Body–midwing (configuration 4)	——	0.00	——

[a] $\lvert XCP_i \rvert$ Absolute value of interaction center of pressure.
[b] Nose-down moment.
[c] Nose-up moment.

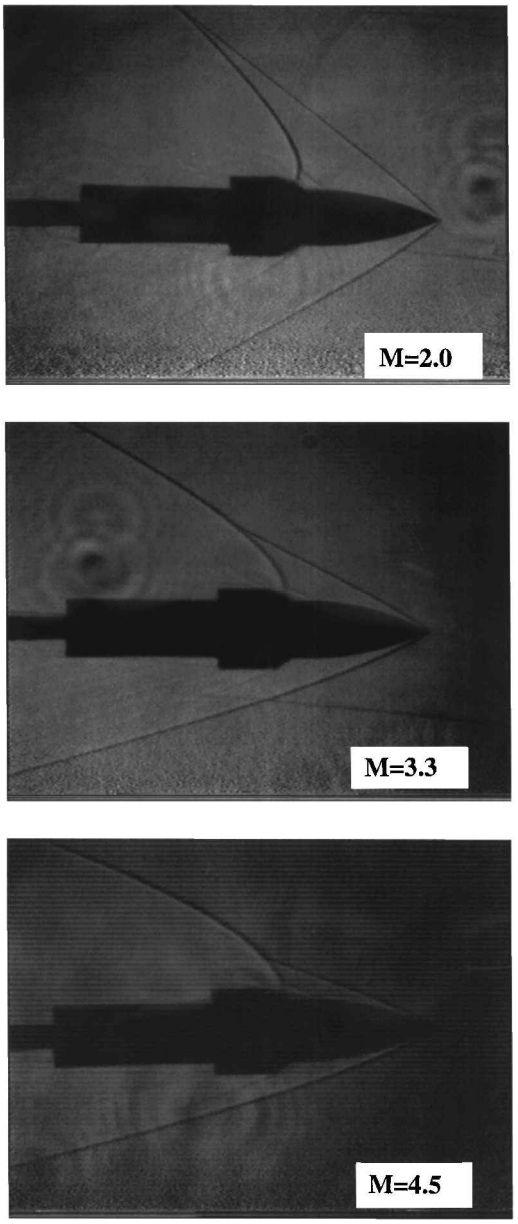

Fig. 8 Schlieren photographs for supersonic Mach 2, 3.3, and 4.5: configuration 1.

the flowfield for the three Mach numbers 2, 3.3, and 4.5 at nearly zero angle of attack. The jet-to-tunnel dynamic pressure ratio (Q_j/Q_t) is similar for the three cases, but the stagnation pressure ratio (P_{0j}/P_{0t}) varies.

The interaction of the jet bow shock with the nose shock is clearly seen. The separation region ahead of the jet may be discerned in the $M = 2$ photograph. Note the upstream bulging of the jet bow shock for $M = 2$ and the similarity in the intersection location of the shock waves for the three cases.

Discussion and Conclusion

In the present work, lifting surfaces were mounted in the vicinity of the jet nozzle to increase the force amplification. In past research, only marginal force amplification was obtained for bodies of revolution at zero angle of attack. By adding planar surfaces to those bodies, dramatic improvement of the force amplification parameter was obtained in most cases. The present results show sensitivity to the location of the surfaces, the flow Mach number, and the jet injection pressure.

Positive force amplification resulted whenever the lifting surfaces were placed in the vicinity of the jet. Locating such surfaces downstream of the jet nozzle resulted in significant decrease in the amplification factor K for low Mach numbers. In general, large amplification factors were measured for the wings and for the strakes configurations in the vicinity of zero angle of attack. At $M = 4.5$, values of $1.4 < K < 1.6$ were obtained at the injection pressures of 565 psi. This contrasts with $K \sim 1$ for the body alone. For the body–wing combination, similar high amplifications also were obtained at $M = 2$. This should be contrasted with $K \sim 0.7$ for body alone at $M = 2$. Tail-mounted surfaces resulted in control-force losses at $M = 2$, with values of K below those for the body-alone case. Highest force amplification factors at supersonic speeds were obtained for the forward wing surfaces (configuration 1).

In hypersonic flow the force amplification obtained generally exceeded the supersonic values. At $M = 8$, the largest values of $K (K > 2.5)$ were obtained for the configuration with strakes, with the body–wing–tail configuration in second place and the body–wing only the third best. In contrast to the supersonic cases, at hypersonic speeds the downstream parts of the configuration have been shown to give a positive contribution to the force amplification. From the pressure transient experiments it is clear that highest amplification factors are obtained at low-pressure ratios, especially at $M = 8$. Therefore, for lower jet pressures, values of K higher than those presented in Table 2 are obtained. There is an indication of a maximum value of K occurring at $P_{0j}/P_{0t} \sim 1$ for the configuration with wings.

Generally, very low pitching moments (centered at the nozzle) were measured for the forward-wing configurations. For all configurations, the pitching moments were manageable for $M = >4.5$. Relatively strong nose-down pitching moments were obtained for configurations with tail surfaces at $M = 2$. The evidence of this is the large shift in the nozzle location necessary to cancel this interaction moment. At the hypersonic Mach number, nose-up interaction moments were obtained for configurations with strakes and with tail surfaces. This is further evidence of high pressures acting at the downstream parts of the configuration at such velocities. The pitching moment was also found to be dependent on the injection pressure. In general, the pitching moment varies inversely with the jet pressure. Within the yaw plane, it is shown that the force and moment interaction is sensitive to the side slip angle. In conclusion, by properly choosing the lifting surface shape and location and by selecting a conveniently low injection pressure, large force amplification factors can be realized. In addition, significant moments in the desired direction can often be obtained, thus facilitating an aerodynamic contribution in addition to the direct jet plus interaction control force. This aerodynamic contribution, even when the jet force acts through the center of moments, was shown to be of magnitude comparable to the jet thrust. Total control forces three times the magnitude of the jet thrust can, thus, realistically be obtained.

Acknowledgments

This research was sponsored jointly by Defense Research and Development–Mafat and RAFAEL.

References

[1] Spaid, F. W., and Zukoski, E. E., "A Study of Interaction of Gaseous Jets from Transverse Slots with Supersonic External Flows," *AIAA Journal*, Vol. 6, No. 2, 1968, pp. 205–212.

[2] Spaid, F. W., "Two-Dimensional Jet Interaction Studies at Large Values of Reynolds Numbers," *AIAA Journal*, Vol. 13, No. 11, 1975, pp. 1430–1434.

[3] Gillman, B. G., "Control Jet Investigation," *Journal of Spacecraft and Rockets*, Vol. 8, No. 4, 1971, pp. 334–339.

[4]Brandeis, J., "Numerical Study of Jet Interaction at Super and Hypersonic Speeds for Flight Vehicle Control," *18th Congress, International Council of the Aeronautical Sciences* (Bejing, PRC), AIAA, Washington, DC, 1992, pp. 1847–1858 (ICAS Paper 92-4-9.1).

[5]Brandeis, J., and Gill, J., "Experimental Investigation of Side Jet Steering for Missiles at Supersonic and Hypersonic Speeds," *Journal of Spacecraft and Rockets*, Vol. 33, No. 3, 1996, pp. 346–352; also AIAA Paper 95-0316, Jan. 1995.

[6]Yeneriz, M. A., Davis, J. S., Cooper, G. K., and Harvey, D. W., "Comparison of Calculation and Experiment for a Lateral Jet from a Hypersonic Cross-Flow," AIAA Paper 89-2548, July 1989.

[7]Hsieh, T., and Wardlaw, A. B., Jr., "Numerical Simulation of Cross Jet in Hypersonic Flow over a Biconic Body," AIAA Paper 94-0165, Jan. 1994.

[8]Champigny, P., and Lacau, R. G., "Lateral Jet Control for Tactical Missiles," AGARD Special Course on Missile Aerodynamics, N95-14448, von Kármán Inst., Rhode-Saint-Genese, Belgium, June 1994.

[9]Srivastava, B., "Lateral Jet Control of Supersonic Missile: CFD Prediction and Comparison to Force and Moment Measurements," AIAA Paper 97-0639, Jan. 1997.

J. R. Maus
Associate Editor